

Magnetic catalysis and inverse magnetic catalysis in QCD

Niklas Mueller¹ and Jan M. Pawłowski^{1,2}

¹*Institut für Theoretische Physik, Universität Heidelberg, Philosophenweg 16, 69120 Heidelberg, Germany*

²*ExtreMe Matter Institute EMMI, GSI Helmholtzzentrum für Schwerionenforschung mbH, Planckstr. 1, D-64291 Darmstadt, Germany*

We investigate the effects of strong magnetic fields on the QCD phase structure at vanishing density by solving the gluon and quark gap equations, and by studying the dynamics of the quark scattering with the four-fermi coupling. The chiral crossover temperature as well as the chiral condensate are computed. For asymptotically large magnetic fields we find magnetic catalysis, while we find inverse magnetic catalysis for intermediate magnetic fields. Moreover, for large magnetic fields the chiral phase transition for massless quarks turns into a crossover.

The underlying mechanisms are then investigated analytically within a few simplifications of the full numerical analysis. We find that a combination of gluon screening effects and the weakening of the strong coupling is responsible for the phenomenon of inverse catalysis. In turn, the magnetic catalysis at large magnetic field is already indicated by simple arguments based on dimensionality.

PACS numbers: 11.15.Tk, 11.30.Rd, 12.38.Aw, 12.38.Gc

I. INTRODUCTION

In recent years there has been a growing interest in the QCD phase structure in the presence of strong magnetic fields, see e.g. [1–8]. Such fields may play an important role for the physics of the early universe, in compact stars, and in non-central heavy ion collisions [4, 7, 9, 10].

Despite the rich phenomenology, theoretical predictions are challenging. Starting from QED, e.g. [11–14] the influence of magnetic fields onto QCD was investigated in both model calculations, e.g. [15–29], such as quark-meson, Nambu–Jona-Lasinio models and AdS/QCD, e.g. [30–36], with functional renormalisation group methods, e.g. [37–43], Dyson–Schwinger equations, e.g. [6, 44–46] and in lattice calculations, e.g. [47–53].

The importance of magnetic fields for chiral symmetry breaking has been pointed out in [11]. It has been argued that chiral symmetry breaking is enhanced due to an effective dimensional reduction, the *magnetic catalysis*. This effect has been linked to an increase of the chiral condensate as well as that of the critical temperature T_c in model studies. Recent lattice results, [47–49, 53], have shown that while the chiral condensate indeed is increased, the critical temperature is decreasing with an increasing magnetic field, at least for small enough magnetic field strength. This effect has been called *inverse magnetic catalysis* or *magnetic inhibition*, [54].

Continuum studies have mainly been performed in low energy fermionic models, such as the (Polyakov loop enhanced) quark-meson- or NJL-model. Hence the reason for the discrepancy has to relate to the full dynamics of QCD, and in particular the back-reaction of the matter sector to the gluonic fluctuations. There have been a number of improvements to these model studies to include QCD dynamics [24, 26–28, 55, 56]. Input parameters of low energy effective models, such as the four-fermi coupling, should be determined from the QCD dynamics at larger scales. At these scales they are sensitive to sufficiently large external parameters such as temper-

ature, density, or magnetic fields. This has been emphasized and used in functional renormalisation group (FRG) studies, see [57–60]. The dependence of the four-fermi coupling on temperature and magnetic field effects including gluon screening has been investigated in the recent FRG-work [43] of QCD in strong magnetic fields, where inverse magnetic catalysis at small magnetic fields and a *delayed magnetic catalysis* at large fields was found, see also [36] for an AdS/QCD computation.

In the present work we investigate (inverse) magnetic catalysis by solving the coupled quark and gluon gap equations within the Dyson–Schwinger (DSE) approach to QCD, and within a FRG study of the four-fermi coupling based on QCD flows and low energy effective models. We find magnetic catalysis at large magnetic fields, while inverse magnetic catalysis takes place at small magnetic fields.

The present work is organized as follows: The gap equations for quark and gluon propagators at finite temperature and magnetic field in two flavor QCD are discussed in Section II. We discuss the dependence of the chiral transition temperature T_c on the magnetic field as well as the magnetic field dependence of the chiral condensate. In Section III the mechanisms behind the phenomena of magnetic and inverse magnetic catalysis are evaluated within analytically accessible approximations to the gap equations as well as to the dynamics of the four-fermi coupling. In this set-up we are also able to reproduce the lattice results at $eB < 1 \text{ GeV}^2$. In summary this provides a complete picture of chiral symmetry breaking in the presence of magnetic fields in QCD.

II. CHIRAL SYMMETRY BREAKING IN LARGE MAGNETIC FIELDS

We investigate chiral symmetry breaking in the presence of large magnetic fields within a functional continuum approach. To this end we calculate the chiral con-



FIG. 1: Quark Dyson-Schwinger equation. Lines with blobs stand for fully dressed propagators, vertices with large blobs stand for fully dressed vertices. Lines without blobs stand for classical propagators, vertices with small blobs stand for classical vertices.

densate for the two lightest quark flavors and obtain the critical temperature T_c at finite magnetic field. This is done by solving the gap equations for the quark and gluon propagator in the presence of a magnetic field using the Ritus method [61–67]. The computations are performed in the Landau gauge.

A. Quark and gluon gap equations

The gap equation for the quark propagator, see Fig. 1, depends on the gluon propagator and the quark-gluon vertex. The former is expanded about the quenched propagator. This expansion has been successfully used at vanishing temperature, e.g. [68, 69], and at finite temperature in e.g. [70–73], the reliability of this expansion has been discussed in [74]. The quark-gluon vertex is estimated with the help of Slavnov-Taylor identities (STIs) from the quark and gluon propagators. The systematic error of the latter estimate gives rise to the dominating systematic error, at vanishing temperature this has been investigated in [75], a related upgrade of the vertex will be used in a subsequent work.

The inverse quark and gluon propagators, $G_q(q)$ and $G_A(q)$ respectively, read in a tensor decomposition at finite eB and T

$$G_q^{-1}(q) = Z_q(q) (i\gamma_3 q_3 + i\gamma_0 q_0 Z_0 + i\gamma_\perp q_\perp Z_\perp + M) ,$$

$$G_A^{-1\mu\nu}(q) = \left(Z_\parallel P_\parallel^{\mu\nu} + Z_\perp P_\perp^{\mu\nu} \right) q^2 + \frac{1}{\xi} \frac{q^\mu q^\nu}{q^2} , \quad (1)$$

with $P_\parallel^{\mu\nu} = (g_\parallel^{\mu\nu} - p_\parallel^\mu p_\parallel^\nu / p_\parallel^2)$ and $P_\perp = P - P_\parallel$, where $P_\perp^{\mu\nu}$ is the transverse projector. The projection operator $g_\parallel^{\mu\nu}$ has the property $g_\parallel^{\mu\nu} p_\parallel^\mu = p_\parallel^\nu$. The Ritus representation Eq. (1) for the quark propagator is equivalent to the Schwinger proper time method, see e.g. [76]. In the following we will denote $Z_A \equiv Z_\parallel$ and concentrate on the Landau gauge, $\xi = 0$. The STIs-induced parametrisation of the quark-gluon vertex is introduced as

$$\Gamma^\mu(q, p) = \gamma^\mu z_{\bar{q}Aq}^{\text{DSE}}(q, p) , \quad (2)$$

with $z_{\bar{q}Aq}^{\text{DSE}}(q, p)$ discussed in Appendix A. The quark gap

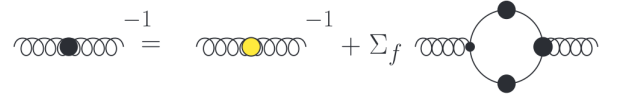


FIG. 2: Gluon Dyson-Schwinger equation. The gluon line with the yellow dot represents the pure glue loops.

equation can be written in a compact notation as

$$G_q^{-1}(p) = G_{q,0}^{-1}(p) + C_f \int_q (g\gamma^\mu) G_q(q) \Gamma^\nu(q, p) G_A^{\mu\nu}(q') , \quad (3)$$

with $q' = q - p$ and $G_{q,0}$ as the bare propagator. The integration \int_q stands for an integration over momenta, as well as sums over Matsubara frequencies and Landau levels. The gluon propagator can be expanded about its pure glue part,

$$G_A^{-1\mu\nu}(p) = G_{\text{glue}}^{-1\mu\nu}(p) + \Pi_f^{\mu\nu}(p) , \quad (4)$$

where we have written the fermionic part of the gluon self energy explicitly, while the gluon and ghost loop contributions are contained in G_{glue} . The corresponding DSE for the gluon propagator within this expansion is depicted Fig. 2. In the following we consider the back-reaction of the vacuum polarisation on the pure glue part as small, and approximate

$$G_{\text{glue}}^{-1\mu\nu}(p) \approx G_{\text{YM}}^{-1\mu\nu}(p) . \quad (5)$$

At vanishing temperature this has been shown to hold quantitatively for momenta $q \gtrsim 4$ GeV, while for smaller momenta this approximation still holds qualitatively with an error of less than 20%, see Fig. 6 in [74]. Note that for momenta $q \gtrsim 4$ GeV the dominant effect of the unquenching is the modification of the scales ($\Lambda_{\text{YM}} \rightarrow \Lambda_{\text{QCD}}$) and the momentum dependence induced by the different β -functions. This is well-captured with the above procedure. In turn, at lower momentum scale the non-perturbative mass-gap related to confinement comes into play. The magnetic field leads to a shift in the momentum dependence such as that of the running coupling, as well as (additional) mass-gaps in propagators. For both asymptotic regimes ($eB \rightarrow 0$ and $eB \rightarrow \infty$) these effects are well-captured semi-perturbatively and we expect that the approximation (5) holds well. For the intermediate regime we rely on the error estimate at zero temperature of about 20% deduced from [74].

The fermionic vacuum polarisation part $\Pi_f^{\mu\nu}(P)$ reads

$$\Pi_f^{\mu\nu}(p) = \frac{1}{2} \text{tr} \int_q (g\gamma^\mu) G_q(q) \Gamma^\nu(q, p) G_q(q') , \quad (6)$$

where the trace includes a sum over the quark flavors. Details of this expansion can be found in [6]. Here we proceed in the lowest Landau level approximation, where

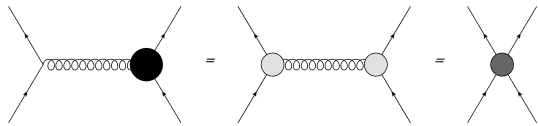


FIG. 3: Relation of the quark DSE interaction kernel to a 1PI skeleton expansion, which in effect induces an effective momentum dependent four-fermi vertex.

we write down the most general tensor decomposition for gluon and quark propagators. Projecting onto different tensor compositions, we obtain a coupled set of equations for the dressing functions of the different tensor components. In the next section we will comment on the relation of the Dyson-Schwinger equations to other functional expansions and discuss the numerical solutions to these equations.

B. Skeleton expansion

Before proceeding to the numerical analysis, we discuss the standard approximation schemes for the quark-gluon vertex used in the Dyson-Schwinger framework from a more general point of view. This allows us to connect the present ansätze to the approximations used in gap equations derived within other functional approaches, such as functional renormalisation group (FRG) or nPI-approaches.

DSE studies have made extensively use of the specific input for the quark-gluon vertex and the YM-gluon propagator in (A2) and (A4) and similar truncations with great success. Since the quark and gluon self energy diagrams, depicted in Fig. 1 and Fig. 2, contain one bare vertex, the correct renormalisation group behavior and momentum dependence of the equations must be discussed carefully. The truncations to the gap equations (3) and (4) can actually be very well motivated from a skeleton expansion of the 1PI effective action, which would yield similar diagrams as in Fig. 1 and Fig. 2, but with both vertices dressed. Fig. 3 serves to strengthen this motivation as it becomes clear that all approximations should encode the correct behavior of the four-fermi interaction, which is at the heart of chiral symmetry breaking. This allows to consistently reshuffle functional dependencies in the interaction kernels of the above equations.

In turn, the FRG-approach (or nPI effective action) can be used to systematically derive gap equations in terms of full propagators and vertices respectively, see e.g. [77]. Here, we simply note that the 1PI effective action can be written as

$$\Gamma[\phi] = \frac{1}{2} \text{Tr} \ln \Gamma[\phi] + \int_t \partial_t \Gamma_k[\phi] - \text{terms}, \quad (7)$$

where ϕ encodes all species of fields, the trace in (7) sums over momenta, internal indices and all species of fields including relative minus signs for fermions (ψ and ψ^\dagger are

counted separately), and a logarithmic RG-scale $t = \ln k$. The RG-scale in (7) is an infrared scale. Momenta $p^2 \lesssim k^2$ are suppressed in $\Gamma_k[\phi]$, and $\Gamma[\phi] = \Gamma_{k=0}[\phi]$. The second term on the right hand side of (7) is a RG-improvement term which only contains diagrams with two loops and more in full propagators and vertices. To see this we discuss the gap equation derived from (7). It follows by taking the second derivative of (7) w.r.t. to the fields. The first term of the right hand side gives the diagrams as in Fig. 1 and Fig. 2 with only full vertices (and additional tadpole diagrams). These diagrams can be iteratively re-inserted into the RG-improvement term, systematically leading to higher loop diagrams in full propagators and vertices. Due to its sole dependence on dressed correlation functions such a diagrammatics naturally encodes the momentum- as well as the RG-running on an equal footing. This also facilitates the consistent renormalisation. Note however that it comes at the price of an infinite series of loops diagrams which can be computed systematically. Here we take the simplest non-trivial approximation which boils down to Fig. 1 and Fig. 2 with only full vertices. In terms of the original gap equation this leads to the relation

$$z_{\bar{q}Aq}^{\text{DSE}} \approx (z_{\bar{q}Aq}^{\text{1PI}})^2, \quad (8)$$

where $z_{\bar{q}Aq}^{\text{1PI}}$ is the dressing function of the 1PI-quark gluon vertex. This immediately leads to the standard DSE-dressing in (A2). Moreover, in our numerical study the vertices are evaluated at their symmetric momentum point.

Note that, while the ansatz for $z_{\bar{q}Aq}^{\text{DSE}}$ is indeed consistent when used in the quark and gluon gap equations, it cannot be used in functional equations for higher vertices such as the four-fermi vertex. It is already clear from the discussion above that a consistent evaluation of renormalisation group running and momentum dependence must be considered separately for each vertex equation.

C. Results

We numerically solve the coupled system of quark and gluon functional equations in the lowest Landau level approximation at finite temperature. This approximation is valid in the presence of a clear scale hierarchy with $eB \gg \Lambda_{\text{QCD}}$. We use an ansatz for Γ^μ similar to that used in Dyson-Schwinger studies, e.g. [6, 78], discussed in appendix A, but adapted for temperature and magnetic field effects.

While at large momentum the influence of temperature and magnetic fields is very small, at large temperatures and magnetic fields the system is effectively dimensionally reduced and hence the momentum dependencies corresponding to the absent dimensions vanish. This can be accounted for if we replace Q_\perp^2 by $2|eB|$ once $Q_\perp^2 < 2|eB|$ and Q_0 by $2\pi T$ for $Q_0 < 2\pi T$ as the relevant scale in the quark gluon vertex, which is consistent with renormali-

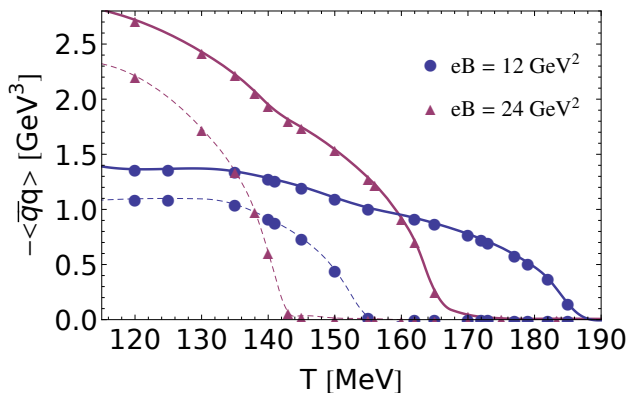


FIG. 4: Comparison of the chiral condensate (scenario 1) for up (continuous lines) and down quark (dashed lines) at $eB = 12 \text{ GeV}^2$ and $eB = 24 \text{ GeV}^2$.

sation group arguments. Within this parametrisation we are still left to decide what exact momentum scale to choose, at which the influence of the external scales T and eB is small already. We investigate this question in detail in section III A.

The gluon propagator deserves some additional attention. It is decomposed in different polarisation components in the presence of an external magnetic field, see e.g. [6]. Apart from the splitting into longitudinal and transverse components with respect to the heat bath, there is an additional splitting transverse and longitudinal to the magnetic field. In the lowest Landau level approximation only the polarisation subspace projected onto by $P_{\parallel}^{\mu\nu} = (g_{\parallel}^{\mu\nu} - p_{\parallel}^{\mu} p_{\parallel}^{\nu} / p_{\parallel}^2)$ receives contributions from the quark loop in the self energy, see [6]. Note that in analogy to temperature effects, also the other gluon components must receive contributions from the interaction with the magnetic field, as gluon and ghost loops mix different polarisation components. This is an important difference between QCD and QED. From dimensionality these contributions are linear in eB at least for asymptotically large magnetic fields, leaving aside implicit B -dependencies via the vertices. Their full computation is beyond the scope of the present work. Here we investigate the following two limiting cases.

1. **Scenario 1** We simply neglect the screening effect of the magnetic field onto those polarisation components that feel magnetic effects only through the Yang-Mills sector in a QED-type approximation. This leads to underestimating the effects leading to inverse magnetic catalysis and hence an upper limit for T_c .
2. **Scenario 2** For the large magnetic fields discussed here, the gluon and ghost loops contributions to the self energy must have a similar dependence on eB as the fermionic part. Since this sector does not directly contain charged particles, the effect of the magnetic field onto the YM-sector is suppressed by powers of the involved couplings. Hence, most

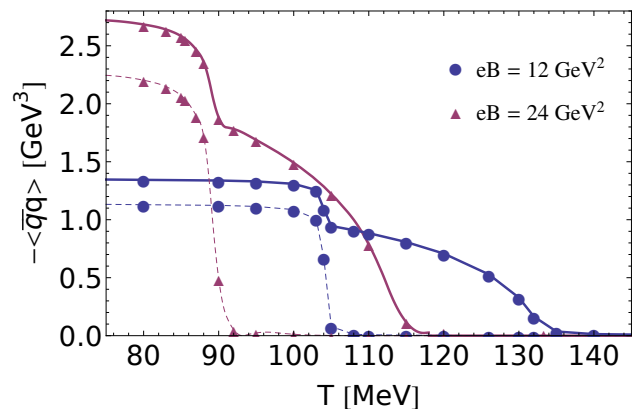


FIG. 5: Comparison of the chiral condensate for scenario 2 at $eB = 12 \text{ GeV}^2$ and $eB = 24 \text{ GeV}^2$.

likely the B -dependence is much smaller than that from the fermionic sector. As a limiting case we will assume the same magnitude of the self energy for all gluon components, which is given by the fermionic contributions. With that we overestimate the gluon screening effect and obtain a lower limit for T_c .

Both scenarios give consistent limiting cases for the truncation used here.

As an order parameter for chiral symmetry breaking we calculate the chiral condensate as a function of temperature and magnetic field in two flavor QCD in the limit of vanishing bare quark masses $m_u \approx m_d \approx 0$. The Ritus method is not reliable for rather small values of $q_f eB$, with $q_f + 2/3$ and $-1/3$ for up and down quark respectively. We expect the lowest Landau level approximation to be a good estimate once $eB \gtrsim 4 \text{ GeV}^2$ (see [6]) which is also the regime where the approximation (5) works well for vanishing temperature.

The numerical computation is very demanding in the vicinity of the phase transition due to the diverging correlation length. This translates into a numerical error in the critical temperature indicated by the error bars in the plots. Fig. 4 and Fig. 5 show the up- and down-quark condensate for different values of eB . The inverse magnetic catalysis effect described in [48, 49] is evident. While the chiral condensate still rises with the external field in the low temperature limit, the transition between chiral broken and symmetric phase drops. This signals inverse magnetic catalysis as observed on the lattice, [47, 48]. Furthermore the phase transition, which is second order at zero magnetic field turns into a crossover with growing eB , even for vanishing bare quark masses. This can be understood as magnetic screening: the magnetic field effectively serves as an infrared cutoff, which inhibits an infinite correlation length.

In the present computation in two-flavor QCD, an even more intricate effect is observed. Up and down quarks come with different electric charges, therefore the presence of a strong electromagnetic field breaks isospin explicitly. This results in a non-degenerate chiral phase

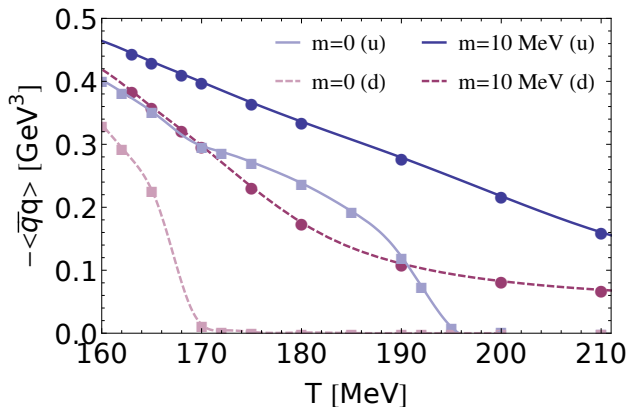


FIG. 6: Comparison of the chiral condensate at zero bare mass and at a finite bare quark mass of $m_u = m_d = 10$ MeV at $eB = 4$ GeV² in scenario 1.

transition for the two flavors. Because gluons travel through a medium filled with both virtual up and down quarks, isospin breaking effects the self interactions of the quarks, which leads to interference between the chiral transitions of the two flavors as seen in Fig. 4 and Fig. 5.

This interference can be interpreted as follows. Virtual quark fluctuations contributing to the gluon screening are suppressed in the chiral broken phase by the quark mass. Since the down quark undergoes the chiral phase transition already at lower scales, its fluctuations are suddenly enhanced due to the vanishing mass in the symmetric phase. The up quark, while still in its chirally broken phase, is drastically affected by these enhanced fluctuations, which lead to reduction of the up quark condensate even below the real phase transition.

It can be seen from Fig. 4 and Fig. 5 that this effect is more prominent in scenario 2, which should come as no surprise, as the coupling of the magnetic field to the gauge sector is probably overestimated here. Nevertheless the isospin induced chiral transition substructure is observable in the limiting scenario 1 as well, which is a strong indication of its validity. Therefore this important physical effect might be observable in lattice calculations, as well. In [48, 49] the averaged chiral condensate was investigated at finite quark mass. However when we investigate the chiral transition at a bare quark mass of 10 MeV we find that the interference effect is completely masked by the crossover behavior as can be seen in Fig. 6. Note that here the unregularized condensate at finite bare mass is plotted, hence the offset between the curves.

In analogy with lattice calculation we define T_c at the inflection points of the curves shown. In Fig. 7 and Fig. 8 the obtained values for T_c for the limiting cases described by scenario 1 and 2 are shown. The two curves give lower and upper limits for T_c , as discussed before. The chiral transition temperature is decreasing for a large range in eB before it seems to saturate for intermediate values in both scenarios. At very large fields it rises again.

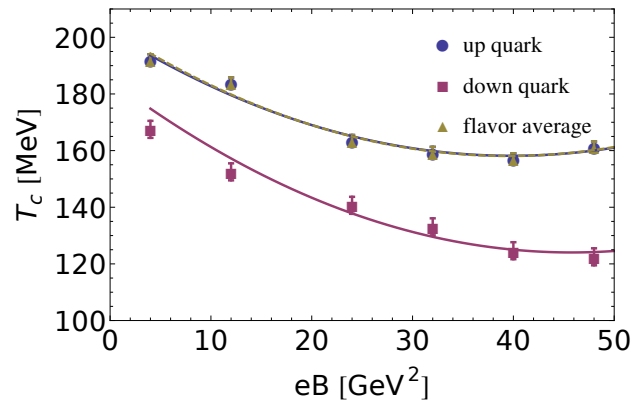


FIG. 7: Critical temperature obtained from scenario 1 for up quark, down quark and from the flavor averaged condensate.

In accordance with our previous discussions we see that the up and down quark chiral transitions do not coincide. The transition temperature from the flavor averaged quark condensate is given in Fig. 7 and Fig. 8 as well. As can be seen from Fig. 4 and Fig. 5 the transition temperature of the flavor averaged condensate is essentially determined by the up quark.

Both scenarios give estimates for the chiral transition temperature, which differ only quantitatively. Scenario 1, which underestimates the magnetic field effects in the gluon sector extrapolates to a critical temperature at $eB = 0$ between 170 – 210 MeV with a turning point between catalysis and inverse catalysis of about $eB \approx 30$ GeV². On the other hand scenario 2 gives T_c at zero magnetic field of about 140 – 165 MeV with a turning point slightly higher than in scenario 1. This is in accordance with the fact that scenario 2 overestimates the gluonic sector, which is the source of the inverse catalysis effects. At $B = 0$ the chiral phase transitions for up and down quark coincide. While the continuous lines in Fig. 7 and Fig. 8 are obtained from a fit with a simple quadratic polynomial, reflecting the turnover behavior at large fields, these should not be mistaken as extrapolations towards zero. Furthermore the computations have been performed in the lowest Landau level approximation. This leads to an uncertainty of about 10% for B smaller than 10 GeV², while the qualitative behavior is not affected, as discussed in [6, 8]. In the following section we will see that the behavior of T_c at small B is steeper than just quadratic.

It is well known that within approximation schemes such as the one discussed here, relative fluctuation scales are usually well accounted for, whereas absolute scales have to be fixed. The position of T_c at $eB = 0$ gives us the possibility of identifying absolute scales and allows to adjust our truncation. We will not be concerned about matching the exact scale of T_c at zero magnetic field with the lattice, moreover we will investigate the mechanisms behind the $B - T$ phase structure in greater detail. We

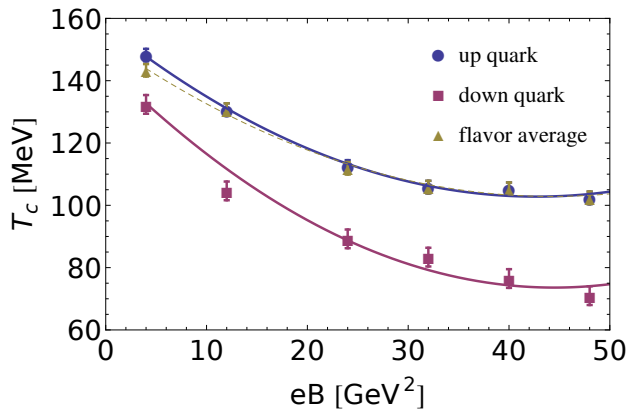


FIG. 8: Critical temperature obtained from scenario 2.

will discuss the issue of scales in the following sections.

III. ANALYTIC APPROACHES

In the present Section we are specifically interested in the mechanisms at work in magnetic and inverse magnetic catalysis. To that end we discuss approximations to the quark gap equation in Section III A, as well as to the dynamics of the four-fermi coupling or quark scattering kernel in Section III B, that allow for an analytic approach to chiral symmetry breaking. While the quark gap equation can be straightforwardly reduced to an analytic form from that used for the numerical study, the four-fermi coupling is studied in a renormalisation group approach to QCD, that reduces to an NJL-type model for low momentum scales.

A. Quark gap equation

The mechanisms behind the phenomena observed in our numerical study can be analyzed within approximations detailed below, that allow for an analytic access. These approximations to the gap equation have been introduced in [13] for QED, and can be extended to QCD at finite temperature. The self-consistent Dyson-Schwinger equation for the mass functions reads in lowest Landau level approximation with zero bare mass

$$M(p_{\parallel}) = 4\pi C_F \sum_{q_{\parallel}} \frac{M(q_{\parallel}) \text{Tr}(\Delta(\text{sgn}(eB)) \gamma_{\parallel}^{\mu} \gamma_{\parallel}^{\nu})}{M^2(q_{\parallel}) + q_{\parallel}^2} \int_{k_{\perp}} \alpha_s \exp\left(-\frac{k_{\perp}^2}{2|eB|}\right) \frac{P_{\mu\nu}(k)}{k^2 + \Pi(k^2)}. \quad (9)$$

Here $\int_{k_{\perp}} = T \sum_n \int dq_{\parallel} / (2\pi)^3$ and $\Delta(s) = (1 + s\sigma^3)/2$. The quark gap equation (9) is obtained from a skeleton expansion of the effective action, e.g. [79], and is nothing

but a manifestly renormalisation group invariant approximation of the above Dyson-Schwinger equations, see the discussion in Section II B. It includes only dressed vertices. In appendix A we discuss how the interaction kernels can be related in both pictures. The 1PI quark-gluon vertex is parametrized as

$$\Gamma_{\bar{q}Aq}^{\mu}(q^2) = Z_A^{1/2}(q^2) \sqrt{4\pi\alpha_s(q^2)} \gamma_{\parallel}^{\mu}, \quad (10)$$

The gluon propagator is transversal due to the Landau gauge, and we allow for a gluonic mass via thermal and magnetic effects. $M(p_{\parallel})$ is a function that is approximately constant in the IR but falls off rapidly for $p_{\parallel}^2 \geq 2|eB|$. Hence, if we are interested in $M(0) = M_{\text{IR}}$ we can write, dividing the equation by its trivial solution,

$$1 - 4\pi^2 C_F T \sum_{q_{\parallel}}^{2eB} \frac{1}{M_{\text{IR}}^2 + q_{\parallel,f}^2} \times \int dx \frac{\alpha_s \exp(-x/2|eB|)}{q_{\parallel,b}^2 + x + \Pi(x, q_{\parallel,b})} \left(2 - \frac{q_{\parallel,b}^2}{q_{\parallel,b}^2 + x}\right) = 0. \quad (11)$$

In (11) we have introduced $q_{\parallel,b} \equiv (q_3, 2n\pi T)$ and $q_{\parallel,f} \equiv (q_3, 2\pi T(n + 1/2))$. Chiral symmetry breaking is realized once a solution $M_{\text{IR}}^2 > 0$ exists. Due to the shape of $M(q)$ and the exponential factor in (11), the integrand only has support for $x \lesssim 2|eB|$. In the following we carefully investigate the ingredients to this self consistent equation and the physical mechanisms, which are responsible for the intriguing behavior seen in the previous section.

Due to the finite support of the integrand, the momenta running through the vertices are comparable or smaller than the relevant dimensionful quantities eB and T^2 . Note that in our numerical study we have used an ansatz for the quark gluon vertex, that includes generic eB and T dependencies. Here we utilize the fact that the running of α_s is dominated by the temperature and magnetic field scales. We resort to a simple ansatz for $\alpha_s(Q^2/\Lambda_{\text{QCD}}^2)$ based on the analytic coupling $\alpha_{s,\text{HQ}}$ suggested in [80, 81], see [82] for an investigation within the present context. This coupling yields a linear potential such as seen in the heavy quark limit.

$$\alpha_s(z) = \alpha_{s,\text{HQ}}(z) r_{\text{IR}}(z), \quad (12)$$

where

$$\alpha_{s,\text{HQ}}(z) = \frac{1}{\beta_0} \frac{z^2 - 1}{z^2 \log(z^2)}, \quad (13)$$

with $\beta_0 = (33 - 2N_f)/12\pi$ and

$$z^2 = \frac{\lambda_B 2eB + \lambda_T (2\pi T)^2}{\Lambda_{\text{QCD}}^2}, \quad (14)$$

with coefficients λ_T, λ_B , which are of order one. These

coefficients determine the point at which eB or T dominate momentum scales. For the relevant magnetic fields and temperatures the running of the coupling with temperature is very small compared to the running with eB . We use an ansatz for the infrared behavior of the vertex, which is parametrized in r_{IR} . Here we use

$$r_{\text{IR}}(z^2) = \frac{z^4}{(z^2 + b^2)^2} \left(1 + \frac{c^2}{z^2 + b^2} \right), \quad (15)$$

which scales with $\propto z^4$ for $z \rightarrow 0$, and approaches unity in the perturbative regime. Eq. (12) reproduces the correct behavior of the full quark gluon vertex in (10). We leave b and c as parameters which allow us to model the infrared behavior of the quark gluon vertex. Our ansatz for (15) is motivated from the quantitative renormalisation group study of quenched QCD in [75], which we use to determine b and c . We get

$$b = 1.50, \quad c = 7.68, \quad (16)$$

from the fit to Fig. 4 in [75].

Furthermore we discuss the gluon self energy in the presence of magnetic fields at finite temperature in this simplified setup. It is important to notice that we can facilitate our calculations by the following argument. The function on the right hand side of (11) is a continuous real function of M_{IR} and approaches +1 as $M_{\text{IR}} \rightarrow \infty$. Hence it is sufficient to check whether the expression is negative for $M_{\text{IR}} = 0$, because then it had to pass through zero at some point, which means that a solution exists.

The gluon self energy receives two important contributions. The first is through the appearance of fermion loops, which are also present in an abelian calculation. The fermionic self energy part in lowest Landau level approximation with $M_{\text{IR}} = 0$ factorizes

$$\Pi_f^{\mu\nu}(p) = \alpha eB \exp(-p_{\perp}^2/2eB) \Pi^{\mu\nu}(p_{\parallel}, T). \quad (17)$$

Contracting with $P^{\mu\nu}$ in the Landau gauge, we can write the second term as

$$\begin{aligned} \Pi_f(p_{\parallel}, T) &= -8\pi^2 \left[3 - 2(1 - p_{\parallel}^2/p^2) \right] \frac{1}{\tau^2} \\ &\times \int_0^1 dx \sum_{\vec{q}_{\parallel}} \frac{x(x-1)}{(\vec{q}_3^2 + (2\pi)^2(n+1/2)^2 + x(1-x)/\tau^2)^2}, \end{aligned} \quad (18)$$

where we defined $\tau^2 \equiv T^2/p_{\parallel}^2$. The function can be evaluated numerically and is very well described by the simple function

$$\Pi_f(p_{\parallel}, T) = (1/2\pi) \left[3 - 2(1 - p_{\parallel}^2/p^2) \right] \frac{1}{1 + (4\pi^2/3)\tau^2}. \quad (19)$$

Eq. (17) and Eq. (19) state that the relevant contribu-

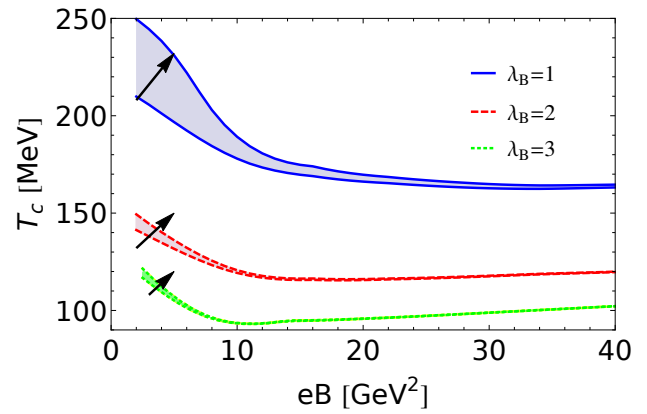


FIG. 9: Analytic calculation of the critical temperature for the chiral phase transition. The bands indicated correspond to $\lambda_T = 1$ and $\lambda_T = 0$. Arrows indicate the direction from $\lambda_T = 1$ to $\lambda_T = 0$.

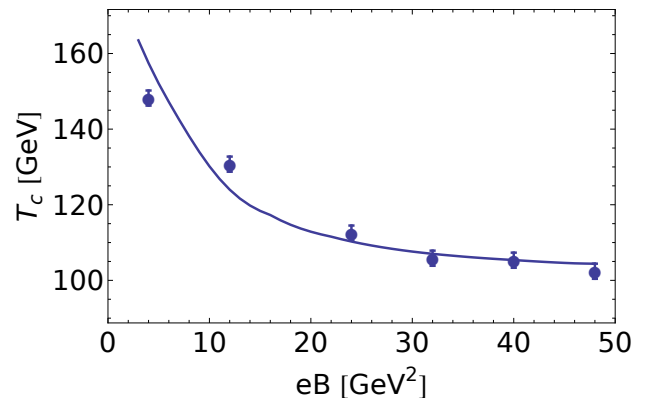


FIG. 10: Comparison of the critical temperature obtained with our full numerical procedure to the simple analytic estimate for $\lambda_B = 1.1$, $\lambda_T = 1$ and $\kappa = 1.19$.

tions to the self energy stem from $p_{\perp}^2 \approx 2eB$ and $p_{\parallel}^2 \approx T^2$. Similar as before, the influence of the magnetic field onto the Yang-Mills sector is not easily accounted for. Here we focus on the abelian-like part of the gluon self energy. As we have investigated before numerically, this is qualitatively correct and we will use Eq. (14) to account for the correct scales. It is well known from Dyson-Schwinger studies [83], that approximations similar to this semi-bare vertex ansatz underestimate the strength of chiral symmetry breaking, due to the negligence of important tensor structures in the vertex, especially those structures that break chiral symmetry explicitly [75]. In order to compensate the overall weakness of the interaction, we allow for a phenomenological parameter κ in front of the integral in Eq. (11).

Using our simple ansatz we can investigate chiral symmetry. In Fig. 9 a family of solutions to Eq. (11) is shown for various values of λ_B and λ_T , using the ansatz described above with $\kappa = 1.2$ for the two upper curves and $\kappa = 1.4$ for the lower curves. The choice of κ is for better

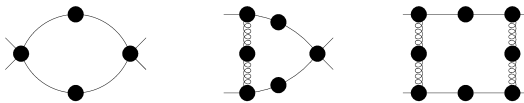


FIG. 11: Diagrams contributing to the renormalisation group flow of the four-fermi coupling.

visualisation only, as the curves can be shifted up and down using this parameter.

The observed behavior agrees with that in our numerical study. It can be seen from Fig. 9, that for small eB inverse magnetic catalysis is present, while at large eB the critical temperature rises again with the magnetic field, with

$$T_c(B/\Lambda_{\text{QCD}}^2 \rightarrow \infty) \propto \sqrt{eB}, \quad (20)$$

as one would anticipate from dimensional considerations. This behavior is universal for all λ_B and λ_T . We see that the choice of λ_B effects the position of the turning point of the chiral phase boundary.

With the present analytical considerations the numerical results in Fig. 7 and Fig. 8 are readily explained: they roughly correspond to $\lambda_B \approx 1$, which explains the relatively large value of eB at the turning point. We see that already small changes in λ_B have a huge effect on this quantity, see Fig. 9.

In Fig. 10 we have plotted the analytic result with $\lambda_B = 1.1$, $\lambda_T = 1$ and $\kappa = 1.19$, which agrees well with the numerical results from scenario 2. Based on the present work we estimate that $\lambda_B \approx 2 - 3$ is a realistic choice for the B -dependence of the running coupling, as in our numerical study quark and gluon propagator turn into their corresponding $B = 0$ -propagators at this momentum scale.

The present analysis reveals the following mechanism: The gauge sector acquires a B -dependence through the feedback of the fermionic sector. This dependence is responsible for the phenomena called inverse magnetic catalysis, as has been also observed recently in a FRG-study within QCD, [43]. This also explains why it cannot be seen in model calculation without explicit QCD input. From Eq. (11), Eq. (12) and Eq. (19) we see that the gluon screening and the running of the strong coupling (both by thermal and magnetic effects) are competing with the generic fermionic enhancement of chiral symmetry breaking in a dimensionally reduced system. We see from Fig. 9 that at small magnetic field screening effects dominate the behavior of the fermionic self energy, while at asymptotically large fields, thermal fluctuations are negligible and hence eB , as the dominating scale, drives the phase transition towards higher T_c (magnetic catalysis).

B. Four-fermi coupling

For a further analytical grip we also resort to a low energy effective theory point of view: integrating-out the gapped gluons leads to an effective four-fermi theory, that is initialized at about the decoupling scale of the glue sector of $\Lambda \approx 1$ GeV. Previously there have been phenomenological approaches in low energy effective models to include QCD dynamics as the source of the inverse magnetic catalysis effect [24, 25, 55]. From the point of view of the FRG for QCD this can be seen as follows [60, 70, 74, 75, 84-86]: At a large momentum scale k QCD is perturbative, and the 1PI effective action Γ_k in (7) is well-described perturbatively. A four-fermi coupling is generated from the one-loop diagrams (in full propagators and vertices) encoded in (7), the related diagrams are depicted in Fig. 11. In the present discussion we have dropped diagrams that depend on the $q\bar{q} - AA$ vertex, $qq\bar{q}\bar{q} - AA$ -vertex and the $qq\bar{q}\bar{q}\bar{q}\bar{q}$ -vertex. Furthermore we assume a classical tensor structure for the $\bar{q}Aq$ -vertex with a coupling $\sqrt{4\pi\alpha_{s,k}}$, and only consider the scalar-pseudo-scalar four-fermi vertex

$$\Gamma_{\text{four-fermi}}[q, \bar{q}, B] = \frac{1}{2} \bar{q}_i^{a\alpha} q_j^{b\beta} \Gamma_{k,ijklm}^{abcd} \bar{q}_l^{c\gamma} q_m^{d\delta}, \quad (21)$$

with the scalar-pseudo-scalar tensor structure

$$\Gamma_{k,ijklm}^{abcd} = \lambda_k [\delta_{ij}\delta_{lm}\delta^{ab}\delta^{cd} + (i\gamma_5)_{ij}(i\gamma_5)_{lm}(\tau^n)^{ab}(\tau^n)^{cd}]. \quad (22)$$

The four-fermi term in (21) can be viewed as the interaction term of a NJL-type model. Within the approximation to QCD outlined above the flow of the four-fermi coupling, $\partial_t \lambda_k$, has the form

$$\begin{aligned} \partial_t \lambda_k = & -k^2 \lambda_k^2 F_\lambda(G_q) - \lambda_k \alpha_{s,k} F_{\lambda\alpha_s}(G_q, G_A) \\ & - \frac{\alpha_{s,k}^2}{k^2} F_{\alpha_s^2}(G_q, G_A), \end{aligned} \quad (23)$$

with positive coefficients $F_\lambda, F_{\lambda\alpha_s}, F_{\alpha_s}$. The respective diagrams are depicted in Fig. 11. The different classes of diagrams in Fig. 11 depend on combinations of gluon and quark propagators, G_A and G_q respectively.

The four-fermi coupling λ_k in two-flavor QCD at $T = 0$ has been quantitatively computed (including its momentum-dependence) in quenched QCD with the FRG in [75], and in a more qualitative approximation (without its momentum-dependence) in fully dynamical QCD in [74]. The respective results are depicted in Fig. 12. As expected, the couplings have a similar dependence and maximal strength. However, the slope of the coupling in the qualitative computation in the peak regime relevant for chiral symmetry breaking is bigger for the qualitative computation. This can be traced back to the missing momentum-dependencies, whose lack artificially increases the locality in momentum space and in the cutoff scale. Hence, guided by the experience gained

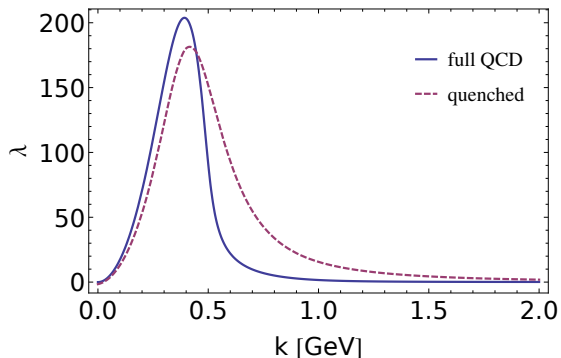


FIG. 12: Scalar–pseudo-scalar four-fermi coupling in the vacuum, $T = 0$, $B = 0$, computed with quantitatively reliable QCD-flows in quenched QCD, [75], and with qualitative full QCD flows, [74].

in the DSE-computations we expect the slope to play a large rôle and we shall use the quantitative quenched results for λ_k and α_s in our present computations. We shall further comment on the differences in the next Section.

For large cutoff scales k the propagators approach the classical propagators. The current quark mass at these scales is negligible and only the cutoff scale is present, if temperature and magnetic field are considered small relative to the cutoff scale. Then the dimensionless F s are simple combinatorial factors. For optimized regulators, [87], they are given as

$$F_\lambda = 4N_c, \quad F_{\lambda\alpha_s} = 12 \frac{N_c^2 - 1}{2N_c}, \quad F_{\alpha_s^2} = \frac{3}{16} \frac{9N_c^2 - 24}{N_c}, \quad (24)$$

in the vacuum, see e.g. [74, 75, 86] for more details. For small enough cutoff scales k the gluonic diagrams decouple due to the QCD mass gap. In the Landau gauge this can be directly seen with the gapping of the gluon propagator. For $T = 0$, $B = 0$ this entails

$$p^2 G_A(p^2 \lesssim \Lambda^2) \propto p^2 / m_{\text{gap}}^2. \quad (25)$$

with $\Lambda \approx 1$ GeV. We emphasize that (25) only reflects the mass gap present in the Landau gauge gluon propagator, the gluon propagator is not that of a massive particle, see e.g. [88]. For momentum scales $p^2 \lesssim \Lambda^2$ this approximately leaves us with an NJL-type model with the action

$$\Gamma_{\text{NJL}}[q, \bar{q}, B] = \int_x \bar{q} i \not{\partial} q + \Gamma_{\text{four-fermi}}[q, \bar{q}, B], \quad (26)$$

with the scalar–pseudo-scalar four-fermi interaction defined in (21). In the presence of a magnetic field this model including fermionic fluctuations has been investigated in [38] within the FRG. Here we shall use the respective results within the lowest Landau level approximation. Then T_c shows an exponential dependence on

the dimensionful parameter eB

$$T_c = 0.42\Lambda \exp\left(-\frac{2\pi^2}{N_c \lambda_\Lambda \sum_f |q_f e B|}\right). \quad (27)$$

The well-known exponential dependence of T_c on the four-fermi coupling λ_Λ already explains the large sensitivity of the scales of magnetic catalysis and inverse magnetic catalysis to details of the computation. Eq. (27) is valid for large magnetic field and for $\Lambda \ll m_{\text{gap}}^2$, that is deep in the decoupling regime of the gluons. An estimate that also interpolates to small magnetic fields is given by

$$T_c = 0.42\Lambda \exp\left(-\frac{1}{c_\Lambda \lambda_\Lambda}\right), \quad (28)$$

with

$$c_k(B) = \frac{N_c}{2\pi^2} \left(\sum_f |q_f e B| + c_1 k^2 \right), \quad \text{with } c_1 = 3, \quad (29)$$

where c_1 has been adjusted to reproduce $T_c(B = 0) \approx 158$ MeV. While Eq. (29) resembles a lowest Landau level approximation, it is actually an expansion in B . Using this ansatz we can describe the behavior of the phase transition on scales below 1 GeV² qualitatively, while the $B = 0$ limit is fixed.

It is also well-known that for $k \gg m_{\text{gap}}$ the flow of the four-fermi coupling is driven by the gluonic diagrams summed-up in F_{α_s} : for large scales we can set $\lambda_{k \gg m_{\text{gap}}} \approx 0$. The gauge coupling is small, $\alpha_{s,k \gg m_{\text{gap}}} \ll 1$ and the flow gives $\lambda_k \propto \alpha_s^2$. This entails that the diagrams with four-fermi couplings are suppressed by additional powers of α_s , and the four-fermi coupling obeys

$$\partial_t \lambda_{\text{glue},k} = -\frac{\alpha_{s,k}^2}{k^2} F_{\alpha_s}(G_q, G_A), \quad (30)$$

where the subscript ‘glue’ indicates that the flow is driven by glue fluctuations. As discussed before, for $k \gg m_{\text{gap}}$ we have classical dispersions for quark and gluon, and the diagrammatic factor F_{α_s} is a constant, see (24). The strong coupling $\alpha_{s,k}$ has the form (12) with $z \propto k$. Integrating (30) with (12) gives

$$\lambda_{\text{glue},k} \propto \frac{\alpha_{s,k}^2}{2k^2} F_{\alpha_s}(G_q, G_A). \quad (31)$$

where an estimate for the B -dependence of the gluonic diagram in F_{α_s} is given in Appendix B.

At vanishing magnetic field $\lambda_{\text{glue},k}$ agrees well with the full result for the four-fermi coupling in [75] for $k \gtrsim 2$ GeV, see Fig. 13. Below $k \approx 2$ GeV, $\lambda_{\text{glue},k}$ is increasingly smaller than the full scalar–pseudo-scalar four-fermi coupling in quenched QCD. In this intermediate range, where all diagrams contribute, we write the resulting cou-

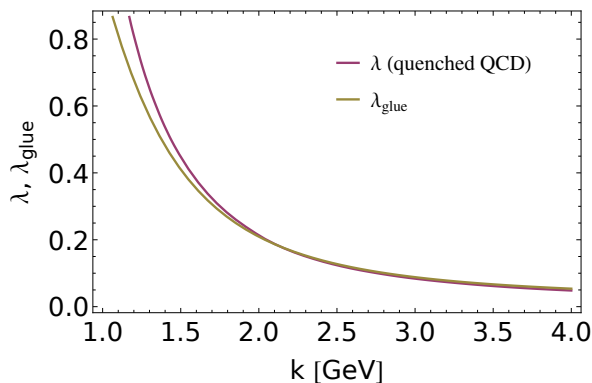


FIG. 13: Scalar–pseudo-scalar four-fermi coupling at $T = 0$, $B = 0$ computed with quantitatively reliable QCD-flows in quenched QCD, [75], in comparison to λ_{glue} computed from (31).

pling within a resummed form that captures already the fermionic diagram proportional to F_λ ,

$$\lambda_k = \frac{\bar{\lambda}_k}{1 - \bar{c}_k \bar{\lambda}_k}, \quad \text{with} \quad \bar{c}_k = \int_k^\Lambda dk' k' F_\lambda(G_q). \quad (32)$$

The resummed form in (32) already reflects the matter part of the flow in (23) which is the term proportional to $\partial_t \lambda_k$. The other terms add up to

$$\partial_t \bar{\lambda}_k = -(1 - \bar{c}_k \bar{\lambda}_k)^2 \left(\lambda_k \alpha_{s,k} F_{\lambda \alpha_s} + \frac{\alpha_{s,k}^2}{k^2} \right). \quad (33)$$

For $\bar{c}_k \bar{\lambda}_k \ll 1$ the flow of $\bar{\lambda}_k$ boils down to (30). For $\bar{c}_k \bar{\lambda}_k \rightarrow 1$ the flow in (33) tends towards zero. In this regime the four-fermi coupling grows large and the matter flow dominates. Hence, for the present qualitative analysis we simply identify $\bar{\lambda}$ with the glue λ_{glue} , (31), up to a prefactor,

$$\bar{\lambda}_k = Z_\lambda \lambda_{\text{glue},k}. \quad (34)$$

The prefactor Z_λ accounts for the fact that we have used results of quantitative QCD-flows [75] for the strong coupling which also includes wave function renormalisations for the quarks. In the current model considerations without wave function renormalisation and further simplifications this has to be accounted for. For the same reason the normalisation 0.42Λ related to a four-fermi flow with an optimised regulator has to be generalised. Moreover, the prefactor $\bar{c}_{\lambda,k}$ is the integrated four-fermi flow already present in (28) up to an overall normalisation accounting for the model simplifications. We choose

$$\bar{c}_k(B) = c_3 c_k(B), \quad \text{and} \quad 0.42 \Lambda \rightarrow 0.42 \Lambda \exp(c_2 - c_3), \quad (35)$$

and arrive at

$$T_c = 0.42 \Lambda \exp \left(-\frac{1}{c_\Lambda \bar{\lambda}_\Lambda} + c_2 \right), \quad (36)$$

with c_Λ as given in (29) and $\bar{\lambda}$ in (34) and (31). Note that the parameter c_3 has dropped out. Its value can be adjusted to achieve a quantitative agreement of (31) with the QCD result in [75] with

$$c_3 = \frac{1}{2Z_\lambda}, \quad (37)$$

where the factor $1/Z_\lambda$ simply removes the mapping factor adjusting for the missing wave function renormalisations in the model computation. This quantitative agreement strongly supports the reliability of the approximate solution to the flow equation given by (32) in the intermediate momentum regime that is of importance for the current considerations. The remaining parameters are fixed as follows,

$$Z_\lambda = 2.2, \quad c_1 = 3, \quad c_2 = 1.4. \quad (38)$$

The parameter c_1 has already been adjusted to meet $T_c(B=0) \approx 158$ MeV, see (28) and (29). The parameter c_2 re-adjusts the overall scale $0.42 \Lambda \rightarrow 0.42 \Lambda \exp c_2 = 1.7 \Lambda$. As already discussed above, it depends on the regulator and the approximation at hand. It reflects the dependence on the renormalisation group scheme. Similarly to c_1 it is fixed with $T_c(B=0) \approx 158$ MeV, and is a function of the overall normalisation of the four-fermi coupling Z_λ . The latter is the only free parameter left. In (38) we use the value that reproduces the lattice results, see Fig. 14. We emphasise that no other parameter is present that allows to shift the minimum in T_c , the latter being a prediction.

Obviously, the effect seen in our numerical and analytic DSE-study, is also present in the analytic approach to the dynamics of the four-fermi coupling, including a direct grip on the underlying mechanisms. We see that the non-monotonous behavior, i.e. the delayed magnetic catalysis, [43, 52], is already present at smaller scales compared to Fig. 7 and Fig. 8, while the lattice results are reproduced.

In turn, for asymptotically large magnetic field, the critical temperature runs logarithmically with B ,

$$T_c(B/\Lambda_{\text{QCD}}^2 \rightarrow \infty) \propto \ln B/\Lambda_{\text{QCD}}, \quad (39)$$

related to a double-log-dependence on B of the exponent. Due to the qualitative nature of the approximation of the B -dependence of the gluon propagator it cannot be trusted for asymptotically large B . Indeed, (39) has to be compared to (20) within the analytic DSE-approach predicting a square root dependence. Note that in the latter computation the quark vacuum polarisation is included selfconsistently at large B even though the backreaction on the pure glue loops in Fig. 2 is neglected. Still this

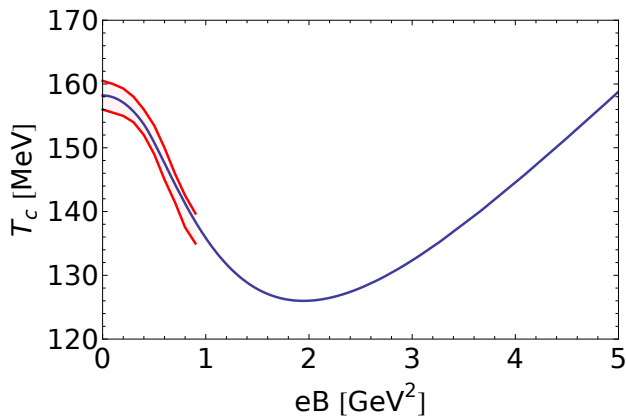


FIG. 14: Comparison of the chiral transition temperature obtained within the simple mean field NJL estimate Eq. (14) to the lattice results of [47] (see their Fig. 10).

indicates the validity of the square root dependence, even though a definite answer to this question requires more work.

C. Discussion of scales & mechanisms

With the findings of the last two sections we have achieved an analytic understanding of the mechanisms at work. The decrease of T_c for small magnetic fields, the increase of T_c for larger fields, as well as the related magnetic field regimes can now be understood. In particular this concerns the magnetic field B_{\min} , where $T_c(B_{\min})$ is at its minimum. This is the turning point between increasing and decreasing $T_c(B)$.

Magnetic catalysis relates to the dimensional reduction due to the magnetic field in diagrams with quark correlation functions leading to an increase of the condensate. At finite temperature the catalysis due to the dimensional reduction is accompanied by a thermal gapping of the quarks that counteracts against the magnetic catalysis effects. In total this leads to a rise of both, the chiral condensate and the critical temperature, if the magnetic field dependence of the involved couplings is sufficiently small. As the magnetic field also sets a momentum scale of the physics involved, this scenario holds true for sufficiently large magnetic field strength $eB/\Lambda_{\text{QCD}}^2 \gg 1$, where the B -dependence of the couplings can be computed (semi-)perturbatively. This explains the regime of delayed magnetic catalysis.

The above discussion of the standard scenario already entails that rapidly changing couplings are required for a decreasing T_c . The couplings involved are the scalar-pseudo-scalar four-fermi coupling λ_k and the strong coupling $\alpha_{s,k}$, where k sets the momentum scale. Both are rising rapidly towards the infrared for momentum scales $k \lesssim 4 - 10$ GeV, for λ_k see Fig. 13. In this regime chiral symmetry breaking and confinement is triggered and

takes place in QCD at vanishing magnetic field. Switching on the magnetic field increases the relevant momentum scale $k^2 \propto eB$ and hence decreases λ and α_s . The condensate still grows with B as the B -enhancement in the broken phase is still present, only T_c decreases.

Our results from the analytic approach to the quark gap equation, presented in Fig. 9, support these findings. The position of the turning point B_{\min} in both the full numerical as well as the analytic analysis of the gap equation depends crucially on the magnetic field and temperature dependence of the quark gluon vertex, see Fig. 9. When contrasted with the quantitative FRG results of α_s in [75], the strong coupling in (A2) decays considerably slower towards the UV. In turn, the couplings in the qualitative FRG study for full QCD, [74] have a steeper decay, for the four-fermi coupling see Fig. 13. Seemingly, this already explains the large value of B_{\min} in the current DSE-study as well as the small value of B_{\min} in [43], which uses approximations similar to [74]. Note however, that we have used the quenched quantitative α_s in the analytic DSE-study which agrees well with the numerical DSE result for $\lambda_B \approx 1$.

In summary we have identified the physics mechanisms behind the $T - B$ phase diagram from our full QCD calculations. Moreover, Fig. 14 suggests a turning point for $eB_{\min} \approx 1.5 - 10$ GeV², the large regime for eB_{\min} being related to the exponential dependence on the couplings. Evidently, the effects observed depend on a sensitive balance of different scales and parameters. Hence, further studies are required to fully uncover the intricate underlying dynamics. Very recent findings in AdS/QCD models, [36], indicate an inverse magnetic catalysis behavior up to $eB \approx 4$ GeV², which supports our findings.

IV. CONCLUSIONS

We have investigated the chiral phase structure of QCD at finite temperature in the presence of an external magnetic field. Our study resolves the discrepancy between recent lattice and continuum calculations at magnetic fields below 1 GeV², see also [43]. We confirm the inverse magnetic catalysis effect seen in lattice studies at small B . At larger B we see that magnetic catalysis is restored, with $T_c \propto \sqrt{eB}$. Indications for the turnover behavior have already been found in [43], and in [52] within two-color lattice-QCD. We hope that further lattice calculations in full QCD at the scales discussed here will become feasible soon.

The reason for this non-monotonous behavior are screening effects of the gauge sector, i.e. modifications of the gluon self energy, as well as the strong coupling α_s in the presence of magnetic fields. Moreover we have investigated the nature of the chiral transition at finite magnetic field.

Apart from the B -dependence of the critical temperature, we observe that the phase transition in the chiral limit turns smoothly into a crossover with rising B . No-

tably, we find a non-degeneracy in the phase transition which is due to the explicit isospin breaking caused by the different electric charges of up and down quark. This non-degeneracy might lead to phenomenological consequences in experimental studies of the QCD phase diagram with non-central heavy-ion collisions, as there might be a mixed phase between the up and down quark transitions. Recent lattice calculations [89] support the possibility of a non-degenerate chiral phase transition.

In addition, our calculations show that, due to this isospin breaking, there is a step-like behavior in the up quark condensate triggered by the chiral transition of the down quark. While this is a significant effect in the chiral limit it smoothens out rapidly with increasing current quark mass. Physical current quark masses are in the transition regime, and this effect might have phenomenological consequences. To our knowledge, this is a novel effect in the QCD phase diagram and it certainly deserves further investigation.

We have used analytic studies of the quark gap equation and the dynamics of the four-fermi coupling for an investigation of the physics mechanisms behind (inverse) magnetic catalysis. The results are discussed at length in the previous Section III C, leading to a rough prediction of the turning point at $eB_{\min} \approx 1.5-10$ GeV. Our investigations highlight the rich phenomenology of QCD matter in external magnetic fields, which motivates further studies, e.g. at finite chemical potential, towards more realistic descriptions of matter under extreme conditions. Recent studies [90] have suggested even richer QCD phase structures in the presence of magnetic fields.

ACKNOWLEDGMENTS

We thank J. Braun, C.S. Fischer, K. Fukushima, W.A. Mian, M. Mitter, S. Rechenberger, F. Rennecke and N. Strodthoff for discussions and work on related subjects. This work is supported by the Helmholtz Alliance HA216/EMMI and the grant ERC-AdG-290623. NM acknowledges support by the Studienstiftung des Deutschen Volkes.

Appendix A: Gluon Propagator and Quark Gluon vertex from Dyson Schwinger studies

Here we discuss the truncation scheme for the quark gap equation and the gluon propagator, based on [71, 78]. The quark gluon vertex is taken as $\Gamma^\mu = z_{qqg}\gamma^\mu$, with

$$z_{qqg}(Q^2) = \frac{d_1}{d_2 + Q^2} \quad (\text{A1})$$

$$+ \frac{Q^2}{\Lambda^2 + Q^2} \left(\frac{\beta_0 \alpha(\mu) \log Q^2 / \Lambda^2 + 1}{4\pi} \right)^{2\delta}, \quad (\text{A2})$$

containing the parameters

$$\begin{aligned} d_1 &= 7.9 \text{ GeV}^2 & d_2 &= 0.5 \text{ GeV}^2, \\ \delta &= -18/88, & \Lambda &= 1.4 \text{ GeV}. \end{aligned} \quad (\text{A3})$$

Here the scales must be identified correctly in order to capture the correct dependence with T and eB . We take Q to be the symmetric momentum $Q^2 = (q^2 + p^2 + (q-p)^2)/3$ at the vertex with $Q^2 = Q_3^2 + Q_0^2 + Q_\perp^2$, where $Q_0^2 = (2\pi T)^2$ if $Q_0^2 < (2\pi T)^2$ and $Q_\perp^2 = 2|eB|$ if $Q_\perp^2 < 2|eB|$. We note that this roughly corresponds to an identification of scales as in section III A with $\lambda_B \approx 1$, although the present vertex is clearly more sophisticated as it includes momentum dependencies and thereby generic eB effects. For a current overview of the quark gluon vertex in Dyson-Schwinger truncations see [91, 92]. Furthermore in order to be able to solve the gluon Dyson-Schwinger equation we rely on lattice input for the Yang-Mills part, which we then "dress" with magnetic field effects, as described above. The reliability of this truncation was already discussed in detail at finite temperature [71] and utilized in the presence of magnetic fields before [6]. The lattice fit is given by

$$\begin{aligned} Z_{\text{YM}}^{-1}(Q^2) &= \frac{Q^2 \Lambda^2}{(Q^2 + \Lambda^2)^2} \left[\left(\frac{c}{Q^2 + a\Lambda^2} \right)^b \right. \\ &\quad \left. + \frac{Q^2}{\Lambda^2} \left(\frac{\beta_0 \alpha(\mu) \log Q^2 / \Lambda^2 + 1}{4\pi} \right)^\gamma \right], \end{aligned} \quad (\text{A4})$$

with

$$\begin{aligned} \Lambda &= 1.4 \text{ GeV}, & c &= 11.5 \text{ GeV}^2, \\ \beta_0 &= 11N_c/3, & \gamma &= -13/22, \end{aligned} \quad (\text{A5})$$

where $\alpha(\mu) = 0.3$ and a and b are temperature dependent parameters, which can be found in [78]. As discussed before the Dyson-Schwinger truncation scheme can be related to the skeleton expansion done in our analytic estimate, which was motivated by renormalisation group invariance

$$4\pi\alpha_s(Q^2)r_{\text{IR}}(Q^2) \frac{P_{\mu\nu}}{Q'^2 + \Pi} \equiv \frac{P_{\mu\nu}}{Z_{\text{YM}}Q'^2 + \Pi_f} z_{qqg}, \quad (\text{A6})$$

where the sum over different polarisation tensor components is implied. The right hand side actually serves as the input to our numerical study, while the different components of Π are determined dynamically from solving the gluon Dyson-Schwinger equation.

Appendix B: Magnetic field dependence of the four-fermi coupling from QCD

As we have discussed in Section III B the value of the NJL coupling λ at the intrinsic cutoff scale of the model

is determined by QCD dynamics. At large scales the dynamics of λ is driven by the rightmost diagram shown in Fig. 11. Within simplifications we will motivate the functional dependence of this diagram on temperature and the magnetic field. In the lowest Landau level ap-

proximation the quarks are constraint to the t-z plane denoted by (\parallel), whereas the gluons propagate in all four dimensions (\parallel, \perp). We write the gluon box diagram in Fig. 11 at zero external momentum as

$$F_{\alpha_s}(eB \geq 0.3 \text{ GeV}) \simeq 4.5 eB \int_0^\infty dq_{\parallel}, \frac{q_{\parallel}}{q_{\parallel}^2 + m_q^2 + \alpha_s eB c_q} \int_0^\infty dq_{\perp}, \frac{q_{\perp}}{[q_{\perp}^2 + q_{\parallel}^2 + m_A^2 + eB\alpha_s c_A]^2}, \quad (\text{B1})$$

where α_s is given as Eq. (12).

For $eB < 0.3$ (B1) is smoothly (quadratic fit) extrapolated to $eB = 0$ with minimising the eB -dependence. The flavor, color and Dirac tensor indices have been contracted, and the comparison with the results for λ in quenched QCD shown in Fig. 13 shows that the prefactor resulting from the tensor contract is approximately 4.5. We have written the propagators in a semi-perturbative form with medium dependent mass terms. Further we have taken $m_A \approx 1$ GeV as the decoupling scale, $m_q \approx 300$ MeV in the chiral broken phase and $c_A = c_q = 1$. Strictly speaking both masses are larger than 1 GeV as we have to add the cutoff masses $\propto \Lambda^2$. We have chosen smaller masses in order to also potentially have access to

the infrared domain $k \rightarrow 0$, where the constituent quark mass is of the order 0.3 GeV and the gluonic mass gap is of the order 1 GeV. Furthermore we have approximated the Matsubara sum by an integration, due to the small level spacing compared to the magnetic field. This approximation does not hold small eB , but (B1) is only used for $eB \geq 0.3$ GeV. Eq. (B1) includes the correct dependence on α_s as well and thus captures eB and T effects qualitatively. The model parameters in Section III B allow us to reproduce the quantitative behavior of the chiral transition temperature and a more elaborate version of Eq. (B1) does not give much greater insight. Apart from the agreement with the T_c results from lattice calculation, Fig. 13 shows that quantitatively reliable results from QCD-flows in quenched QCD [75] are reproduced.

-
- [1] I. A. Shovkovy, Lect.Notes Phys. **871**, 13 (2013), arXiv:1207.5081 [hep-ph].
 - [2] M. D'Elia, Lect.Notes Phys. **871**, 181 (2013), arXiv:1209.0374 [hep-lat].
 - [3] K. Fukushima, Lect.Notes Phys. **871**, 241 (2013), arXiv:1209.5064 [hep-ph].
 - [4] D. E. Kharzeev, L. D. McLerran, and H. J. Warringa, Nucl.Phys. **A803**, 227 (2008), arXiv:0711.0950 [hep-ph].
 - [5] K. Fukushima, D. E. Kharzeev, and H. J. Warringa, Phys.Rev. **D78**, 074033 (2008), arXiv:0808.3382 [hep-ph].
 - [6] N. Mueller, J. A. Bonnet, and C. S. Fischer, Phys.Rev. **D89**, 094023 (2014), arXiv:1401.1647 [hep-ph].
 - [7] J. O. Andersen, W. R. Naylor, and A. Tranberg, (2014), arXiv:1411.7176 [hep-ph].
 - [8] V. A. Miransky and I. A. Shovkovy, (2015), arXiv:1503.00732 [hep-ph].
 - [9] G. Basar, D. Kharzeev, and V. Skokov, Phys.Rev.Lett. **109**, 202303 (2012), arXiv:1206.1334 [hep-ph].
 - [10] G. Basar, D. E. Kharzeev, and E. V. Shuryak, Phys.Rev. **C90**, 014905 (2014), arXiv:1402.2286 [hep-ph].
 - [11] V. Gusynin, V. Miransky, and I. Shovkovy, Nucl.Phys. **B462**, 249 (1996), arXiv:hep-ph/9509320 [hep-ph].
 - [12] V. Gusynin, V. Miransky, and I. Shovkovy, Phys.Rev.Lett. **83**, 1291 (1999), arXiv:hep-th/9811079 [hep-th].
 - [13] V. Gusynin, V. Miransky, and I. Shovkovy, Nucl.Phys. **B563**, 361 (1999), arXiv:hep-ph/9908320 [hep-ph].
 - [14] V. Gusynin, V. Miransky, and I. Shovkovy, Phys.Rev. **D52**, 4747 (1995), arXiv:hep-ph/9501304 [hep-ph].
 - [15] T. Inagaki, D. Kimura, and T. Murata, Prog.Theor.Phys. **111**, 371 (2004), arXiv:hep-ph/0312005 [hep-ph].
 - [16] J. K. Boomsma and D. Boer, Phys.Rev. **D81**, 074005 (2010), arXiv:0911.2164 [hep-ph].
 - [17] M. D'Elia, S. Mukherjee, and F. Sanfilippo, Phys.Rev. **D82**, 051501 (2010), arXiv:1005.5365 [hep-lat].
 - [18] A. J. Mizher, M. Chernodub, and E. S. Fraga, Phys.Rev. **D82**, 105016 (2010), arXiv:1004.2712 [hep-ph].
 - [19] R. Gatto and M. Ruggieri, Phys.Rev. **D82**, 054027 (2010), arXiv:1007.0790 [hep-ph].
 - [20] R. Gatto and M. Ruggieri, Phys.Rev. **D83**, 034016 (2011), arXiv:1012.1291 [hep-ph].
 - [21] B. Chatterjee, H. Mishra, and A. Mishra, Phys.Rev. **D84**, 014016 (2011), arXiv:1101.0498 [hep-ph].
 - [22] R. Gatto and M. Ruggieri, Lect.Notes Phys. **871**, 87 (2013), arXiv:1207.3190 [hep-ph].
 - [23] M. Frasca and M. Ruggieri, Phys.Rev. **D83**, 094024 (2011), arXiv:1103.1194 [hep-ph].
 - [24] M. Ferreira, P. Costa, O. Lourenco, T. Frederico, and C. Providencia, Phys.Rev. **D89**, 116011 (2014), arXiv:1404.5577 [hep-ph].
 - [25] E. Ferrer, V. de la Incera, and X. Wen, (2014), arXiv:1407.3503 [nucl-th].
 - [26] R. Farias, K. Gomes, G. Krein, and M. Pinto, Phys.Rev. **C90**, 025203 (2014), arXiv:1404.3931 [hep-ph].

- [27] A. Ayala, M. Loewe, A. J. Mizher, and R. Zamora, Phys.Rev. **D90**, 036001 (2014), arXiv:1406.3885 [hep-ph].
- [28] A. Ayala, M. Loewe, and R. Zamora, Phys.Rev. **D91**, 016002 (2015), arXiv:1406.7408 [hep-ph].
- [29] L. Yu, J. Van Doorselaere, and M. Huang, (2014), arXiv:1411.7552 [hep-ph].
- [30] O. Bergman, G. Lifshytz, and M. Lippert, JHEP **0805**, 007 (2008), arXiv:0802.3720 [hep-th].
- [31] C. V. Johnson and A. Kundu, JHEP **0812**, 053 (2008), arXiv:0803.0038 [hep-th].
- [32] V. G. Filev, C. V. Johnson, and J. P. Shock, JHEP **0908**, 013 (2009), arXiv:0903.5345 [hep-th].
- [33] F. Preis, A. Rebhan, and A. Schmitt, JHEP **1103**, 033 (2011), arXiv:1012.4785 [hep-th].
- [34] F. Preis, A. Rebhan, and A. Schmitt, Lect.Notes Phys. **871**, 51 (2013), arXiv:1208.0536 [hep-ph].
- [35] A. Ballon-Bayona, JHEP **1311**, 168 (2013), arXiv:1307.6498 [hep-th].
- [36] K. A. Mamo, (2015), arXiv:1501.03262 [hep-th].
- [37] V. Skokov, Phys.Rev. **D85**, 034026 (2012), arXiv:1112.5137 [hep-ph].
- [38] K. Fukushima and J. M. Pawłowski, Phys.Rev. **D86**, 076013 (2012), arXiv:1203.4330 [hep-ph].
- [39] K. Kamikado and T. Kanazawa, JHEP **1403**, 009 (2014), arXiv:1312.3124 [hep-ph].
- [40] K. Kamikado and T. Kanazawa, (2014), arXiv:1410.6253 [hep-ph].
- [41] J. O. Andersen and A. Tranberg, JHEP **1208**, 002 (2012), arXiv:1204.3360 [hep-ph].
- [42] J. O. Andersen, W. R. Naylor, and A. Tranberg, JHEP **1404**, 187 (2014), arXiv:1311.2093 [hep-ph].
- [43] J. Braun, W. A. Mian, and S. Rechenberger, (2014), arXiv:1412.6025 [hep-ph].
- [44] T. Kojo and N. Su, Phys.Lett. **B720**, 192 (2013), arXiv:1211.7318 [hep-ph].
- [45] T. Kojo and N. Su, Phys.Lett. **B726**, 839 (2013), arXiv:1305.4510 [hep-ph].
- [46] P. Watson and H. Reinhardt, Phys.Rev. **D89**, 045008 (2014), arXiv:1310.6050 [hep-ph].
- [47] G. Bali, F. Bruckmann, G. Endrodi, Z. Fodor, S. Katz, *et al.*, JHEP **1202**, 044 (2012), arXiv:1111.4956 [hep-lat].
- [48] G. Bali, F. Bruckmann, G. Endrodi, Z. Fodor, S. Katz, *et al.*, Phys.Rev. **D86**, 071502 (2012), arXiv:1206.4205 [hep-lat].
- [49] Bali, G.S. and Bruckmann, F. and Endrodi, G. and Gruber, F. and Schäfer, A., JHEP **1304**, 130 (2013), arXiv:1303.1328 [hep-lat].
- [50] F. Bruckmann, G. Endrodi, and T. G. Kovacs, JHEP **1304**, 112 (2013), arXiv:1303.3972 [hep-lat].
- [51] Bali, G.S. and Bruckmann, F. and Endrodi, G. and Katz, S.D. and Schäfer, A., JHEP **1408**, 177 (2014), arXiv:1406.0269 [hep-lat].
- [52] E. M. Ilgenfritz, M. Müller-Preussker, B. Petersson, and A. Schreiber, Phys.Rev. **D89**, 054512 (2014), arXiv:1310.7876 [hep-lat].
- [53] V. Bornyakov, P. Buividovich, N. Cundy, O. Kochetkov, and A. Schaefer, Phys.Rev. **D90**, 034501 (2014), arXiv:1312.5628 [hep-lat].
- [54] K. Fukushima and Y. Hidaka, Phys.Rev.Lett. **110**, 031601 (2013), arXiv:1209.1319 [hep-ph].
- [55] E. Fraga, B. Mintz, and J. Schaffner-Bielich, Phys.Lett. **B731**, 154 (2014), arXiv:1311.3964 [hep-ph].
- [56] J. O. Andersen, W. R. Naylor, and A. Tranberg, (2014), arXiv:1410.5247 [hep-ph].
- [57] J. M. Pawłowski, AIP Conf.Proc. **1343**, 75 (2011), arXiv:1012.5075 [hep-ph].
- [58] L. M. Haas, R. Stiele, J. Braun, J. M. Pawłowski, and J. Schaffner-Bielich, Phys.Rev. **D87**, 076004 (2013), arXiv:1302.1993 [hep-ph].
- [59] T. K. Herbst, M. Mitter, J. M. Pawłowski, B.-J. Schaefer, and R. Stiele, Phys.Lett. **B731**, 248 (2014), arXiv:1308.3621 [hep-ph].
- [60] J. M. Pawłowski, Nucl.Phys. **A931**, 113 (2014).
- [61] D. Lee, C. N. Leung, and Y. Ng, Phys.Rev. **D55**, 6504 (1997), arXiv:hep-th/9701172 [hep-th].
- [62] V. Miransky and I. Shovkovy, Phys.Rev. **D66**, 045006 (2002), arXiv:hep-ph/0205348 [hep-ph].
- [63] C. N. Leung and S.-Y. Wang, Annals Phys. **322**, 701 (2007), arXiv:hep-ph/0503298 [hep-ph].
- [64] A. Ayala, A. Bashir, A. Raya, and E. Rojas, Phys.Rev. **D73**, 105009 (2006), arXiv:hep-ph/0602209 [hep-ph].
- [65] E. Rojas, A. Ayala, A. Bashir, and A. Raya, Phys.Rev. **D77**, 093004 (2008), arXiv:0803.4173 [hep-ph].
- [66] V. Ritus, Annals Phys. **69**, 555 (1972).
- [67] V. Ritus, Sov.Phys.JETP **48**, 788 (1978).
- [68] C. S. Fischer, P. Watson, and W. Cassing, Phys. Rev. **D72**, 094025 (2005), arXiv:hep-ph/0509213.
- [69] D. Nickel, R. Alkofer, and J. Wambach, Phys. Rev. **D74**, 114015 (2006), arXiv:hep-ph/0609198.
- [70] J. Braun, L. M. Haas, F. Marhauser, and J. M. Pawłowski, Phys.Rev.Lett. **106**, 022002 (2011), arXiv:0908.0008 [hep-ph].
- [71] C. S. Fischer and J. Luecker, Phys.Lett. **B718**, 1036 (2013), arXiv:1206.5191 [hep-ph].
- [72] C. S. Fischer, L. Fister, J. Luecker, and J. M. Pawłowski, Phys.Lett. **B732**, 273 (2014), arXiv:1306.6022 [hep-ph].
- [73] C. S. Fischer, J. Luecker, and C. A. Welzbacher, Phys.Rev. **D90**, 034022 (2014), arXiv:1405.4762 [hep-ph].
- [74] J. Braun, L. Fister, J. M. Pawłowski, and F. Rennecke, (2014), arXiv:1412.1045 [hep-ph].
- [75] M. Mitter, J. M. Pawłowski, and N. Strodthoff, (2014), arXiv:1411.7978 [hep-ph].
- [76] T.-K. Chyi, C.-W. Hwang, W. Kao, G.-L. Lin, K.-W. Ng, *et al.*, Phys.Rev. **D62**, 105014 (2000), arXiv:hep-th/9912134 [hep-th].
- [77] J. M. Pawłowski, Annals Phys. **322**, 2831 (2007), arXiv:hep-th/0512261 [hep-th].
- [78] C. S. Fischer, A. Maas, and J. A. Müller, Eur.Phys.J. **C68**, 165 (2010), arXiv:1003.1960 [hep-ph].
- [79] C. S. Fischer and J. M. Pawłowski, Phys. Rev. **D80**, 025023 (2009), arXiv:0903.2193 [hep-th].
- [80] A. Nesterenko, Phys.Rev. **D62**, 094028 (2000), arXiv:hep-ph/9912351 [hep-ph].
- [81] A. Nesterenko, Phys.Rev. **D64**, 116009 (2001), arXiv:hep-ph/0102124 [hep-ph].
- [82] N. Christiansen, M. Haas, J. M. Pawłowski, and N. Strodthoff, (2014), arXiv:1411.7986 [hep-ph].
- [83] R. Alkofer, C. S. Fischer, F. J. Llanes-Estrada, and K. Schwenzer, Annals Phys. **324**, 106 (2009), arXiv:0804.3042 [hep-ph].
- [84] J. Braun and H. Gies, JHEP **0606**, 024 (2006), arXiv:hep-ph/0602226 [hep-ph].
- [85] J. Braun and H. Gies, Phys. Lett. **B645**, 53 (2007), arXiv:hep-ph/0512085.

- [86] J. Braun, J.Phys. **G39**, 033001 (2012), arXiv:1108.4449 [hep-ph].
- [87] D. F. Litim, Phys.Lett. **B486**, 92 (2000), arXiv:hep-th/0005245 [hep-th].
- [88] C. S. Fischer, A. Maas, and J. M. Pawłowski, Annals Phys. **324**, 2408 (2009), arXiv:0810.1987 [hep-ph].
- [89] G. Endrodi, (2015), arXiv:1504.08280 [hep-lat].
- [90] K. Nishiyama, S. Karasawa, and T. Tatsumi, (2015), arXiv:1505.01928 [nucl-th].
- [91] R. Alkofer, G. Eichmann, C. S. Fischer, M. Hopfer, M. Vujanovic, *et al.*, PoS **QCD-TNT-III**, 003 (2013), arXiv:1405.7310 [hep-ph].
- [92] R. Williams, (2014), arXiv:1404.2545 [hep-ph].